Journal of Hazardous Materials 177 (2010) 738–742

Contents lists available at ScienceDirect

Journal of Hazardous Materials

journal homepage: www.elsevier.com/locate/jhazmat

Thermal decomposition of 3,4-bis(4′-aminofurazano-3′) furoxan

Wei Zheng*, Jiangning Wang, Xiaoning Ren, Zhiqun Chen, Jun Tian, Yanshui Zhou

Xi'an Modern Chemistry Research Institute, ZhangBa East Road No. 168, Yan Ta District, Xi'an, Shanxi 710065, PR China

ARTICLE INFO

Article history:
Received 2 October 2009
Received in revised form
20 December 2009
Accepted 21 December 2009
Available online 4 January 2010

Keywords:
3,4-Bis(4′-aminofurazano-3′) furoxan (BAFF)
Decomposition kinetics
Thermal decomposition
Differential scanning calorimetry
Thermogravimetry
Fourier transform infrared spectroscopy

ABSTRACT

The thermal decomposition of 3,4-bis(4′-aminofurazano-3′) furoxan (BAFF) was studied by DSC, TG, the combination technique of in situ thermolysis cell with rapid-scan Fourier transform infrared spectroscopy (thermolysis/RSFT-IR) and the fast thermolysis probe with rapid-scan Fourier transform infrared spectroscopy (fast thermolysis/RSFT-IR). The result shows that the melting point of BAFF is 168.4 °C, the peak temperatures of the two exothermic peaks are respectively 260.4 °C and 338.8 °C on DSC curve. The apparent activation energy E_a and the pre-exponential factor A are respectively 122.21 kJ mol^{-1} and $10^{9.89}$ s^{-1} for major exothermic decomposition process of BAFF. The kinetic equation of major exothermic decomposition for BAFF is $d\alpha/dt = 10^{10.07}\exp(-1.46993 \times 10^4/T)(1-\alpha)\,[-\ln(1-\alpha)]^{1/3}$. The thermal decomposition gaseous products of BAFF consist of CO_2, NO_2, N_2O and NO. The BAFF is shown by IR spectroscopy to convert to ammonium dicyanamide ($NH_4[N(CN)_2]$), cyclic azine residues (melamine or melamine-like).

1. Introduction

The furazan or furoxan ring has been found to be a useful substructure for the design of new high density, high energy materials composed exclusively of carbon, hydrogen, nitrogen and oxygen atoms [1,2]. Derivatives of furazan or furoxan are being investigated intensively as they can be thought of to contribute to propellant performance due to high enthalpy of formation of furazan or furoxan ring [3–5].

3,4-Bis(4′-aminofurazano-3′) furoxan (BAFF) is a novel insensitive high energy explosive. Its crystal density is about 1.795 g cm^{-3}. The detonation velocity corresponding to ρ = 1.795 g cm^{-3} is about 8100 m s^{-1}. Therefore, it has the potential for possible use as an energetic ingredient of propellants and explosives. Its preparation and properties have been reported [6,7]. Presently, there are no reports about the thermal decomposition of BAFF.

In the present work, it was studied with regard to the kinetics and the thermal decomposition using differential scanning calorimetry (DSC) and pressure differential scanning calorimetry (PDSC), thermogravimetry and derivative thermogravimetry (TG-DTG). At the same time, the combination technique of in situ thermolysis cell with rapid-scan Fourier transform infrared spectroscopy (thermolysis/RSFT-IR) and the combination technique of fast thermolysis probe with rapid-scan Fourier transform infrared spectroscopy (fast thermolysis/RSFT-IR) were employed to identify the gaseous products and condensed phase products on the thermal decomposition of BAFF.

2. Experimental

3,4-Bis(4′-aminofurazano-3′) furoxan (BAFF) was prepared by our work group. The compound was purified by crystallization from acetone for analysis. Its purity was more than 99.8%. The sample was kept in vacuum desiccators before use.

The tests of differential scanning calorimetry (DSC) were carried out on a differential scanning calorimeter made by US TA instruments, model TA910s. The sample mass is 1–2 mg and a closed aluminum crucible was used as a sample cell. The measurements were performed in a static atmosphere of nitrogen at normal and high pressure. The high pressure was achieved by filling the crucible with nitrogen. Heating was performed at a rate of 10 K min^{-1} except for the determination of kinetic parameters for which the heating rates were 5 K min^{-1}, 10 K min^{-1}, 15 K min^{-1}, and 20 K min^{-1}, respectively.

The experiments of thermogravimetry and derivative thermogravimetry (TG–DTG) were carried out on TGA instrument made by US TA instruments, model TA2950, with sample mass of 2–3 mg in an open aluminum sample cell. The measurements were performed in a dynamic atmosphere of nitrogen with a flow rate of 60 ml min^{-1} and a heating rate of 10 K min^{-1}.

Thermolysis/RSFT-IR measurements were conducted using Model NEXUS 870 FT-IR and in situ thermolysis cell (Xiamen

* Corresponding author. Tel.: +86 02988291702.
E-mail address: zhei_wei035991@yahoo.com.cn (W. Zheng).

0304-3894/$ – see front matter © 2009 Elsevier B.V. All rights reserved.
doi:10.1016/j.jhazmat.2009.12.093

Nomenclature

Symbols and abbreviations

A	pre-exponential factor
BAFF	3,4-bis(4′-aminofurazano-3′) furoxan
DSC	differential scanning calorimetry
DTG	differential thermogravimetry
E	activation energy
$f(\alpha)$	the differential model functions
$G(\alpha)$	the integral model functions
H_o	the total heat effect (corresponding to the global area under the DSC curve)
H_t	the reaction heat at a certain time (corresponding to the partial area under the DSC curve)
Ml	mass lost percentage
PDSC	pressure differential scanning calorimetry
R	the gas constant
r	correlation coefficient
T	temperature (K)
TG	thermogravimetry
T_p	peak temperature
α	conversion degree ($\alpha = H_t/H_o$)
δ	error decided by the equation $\delta = [\varepsilon^2/(n-1)]^{1/2}$
ε	standard deviation
n	the number of data

University, China) with the temperature range of 20–455 K and heating rate of 10 K min^{-1}. KBr pellet samples, well mixed by about 0.7 mg BAFF and 150 mg KBr, were used. Infrared spectra in the 4000–400 cm^{-1} range were acquired by a model DTGS detector at a rate of 11 files min^{-1} and 8 scans file^{-1} with 4 cm^{-1} resolution.

Fast thermolysis/RSFT-IR measurements were made with Model 60SXR FT-IR, in situ thermolysis cell and fast thermolysis probe (CDS instruments corporation) with the temperature range of 20–700 K and heating rate of 700 K s^{-1} (T-jump/RSFT-IR test, heating the sample at a high rate to the constant temperature of 700 K). About 1.0 mg BAFF samples thinly spread on the Nichrome ribbon filament of the probe were used. IR spectra in the 4000–600 cm^{-1} were acquired with a Model MCT-A rapid-scan IR detector at a rate of 5.5 files s^{-1} and 2 scans s^{-1} with 8 cm^{-1} resolution.

3. Results and discussion

3.1. TG

TG/DTG curves and TG–DTG data for BAFF are shown in Fig. 1 and Table 1, respectively. The process can be divided into two main stages as shown in the DTG curve. The first mass loss stage ranges from 181 °C to 269.5 °C, the second mass loss stage ranges from 269.5 °C to 498 °C.

Table 1
TG–DTG data of BAFF (β is 10 K min^{-1}).

The first stage of mass loss	T_{P1} (°C)	Ml_1 (%)	T_{P2} (°C)	Ml_2 (%)
	255.3	45.5	269.5	74.5
The second stage of mass loss	T_{P3} (°C)		Ml_3 (%)	
	330.5		83.3	

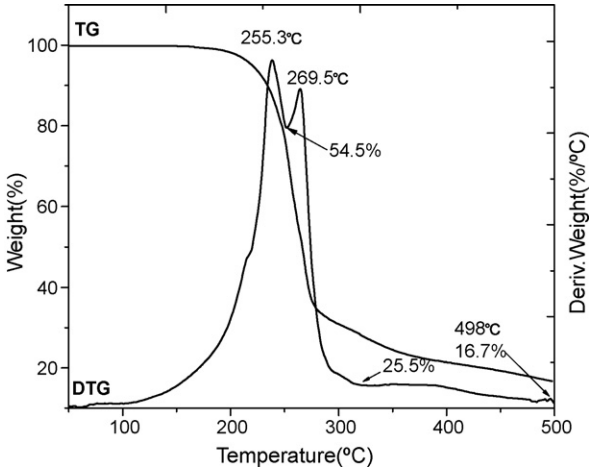

Fig. 1. TG/DTG curve for BAFF at a heating rate of 10 K min^{-1}.

3.2. DSC

The PDSC curves of BAFF at different pressure are shown in Fig. 2.

An endothermic peak at 168.4 °C appears on the DSC curve of the thermal decomposition for BAFF at ambient pressure. Because this temperature approaches the melting point of BAFF (170 °C), the endothermic peak is attributed to the melting of BAFF. There are two exothermic peaks in the DSC curve of BAFF thermal decomposition. The first peak ranges from 181 °C to 291.8 °C with a maximum at 260.4 °C. This is induced by the decomposition of BAFF in molten state, which corresponds to the first stage of mass loss on TG curve. The second peak ranges from 312.3 °C to 385.8 °C. This is induced by the further decomposition of the decomposition products in condensed phase, which corresponds to the second stage of mass loss on TG curve.

From Fig. 3 can be concluded that there is no effect on the molten process of BAFF with the elevated pressure, but obvious effect on the thermal decomposition. The peak temperatures of first decomposition peak of BAFF increase with the elevated pressure. The reason is that an increase in the reactant concentration results from the inhibit effect of pressure on the gasification of molten BAFF. The peak temperatures of second decomposition peak of BAFF decrease with the elevated pressure. The reason is the oxidations strengthen induced by the oxidized gases such as NO_2 and NO.

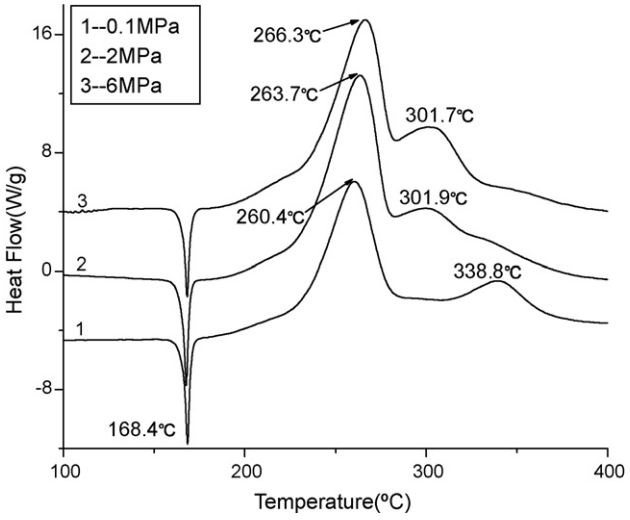

Fig. 2. PDSC curves for BAFF at different pressure (10 K min^{-1}).

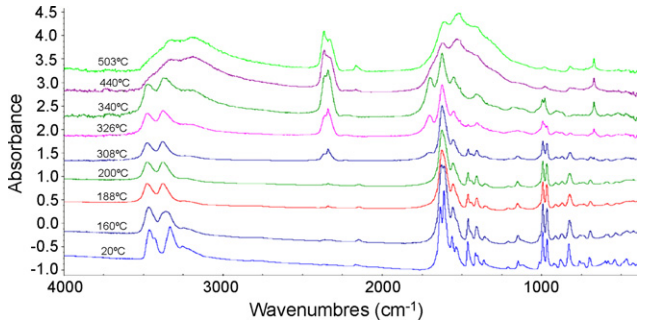

Fig. 3. Infrared spectra of condensed products of BAFF decomposition at different temperature.

Table 2
The DSC peak temperatures (T_p) of BAFF decomposition at various heating rates (β).

β (K min^{-1})	T_{p1} (°C)	T_{p2} (°C)
2.5	236.5	320.9
5	247.3	332.5
10	260.7	333.6
20	271.6	357.5

Table 3
The kinetic parameters obtained from Kissinger and Ozawa methods.

Stage	E_k (kJ mol^{-1})	lg A_k (s^{-1})	E_o (kJ mol^{-1})	r_k	r_o
First	125.88	10.29	128.04	0.999	0.999
Second	160.12	11.52	161.96	0.929	0.937

3.3. Thermal decomposition kinetics

In order to obtain the kinetic parameters [apparent activation energy (E) and pre-exponential factor (A)] of the major exothermic decomposition reaction for BAFF, the Kissinger's method [8] and Ozawa's method [9] were employed. The values of E and A were obtained by the Kissinger's method (with a subscript of k) and Ozawa's method (with a subscript of o) with a multiple heating rate method. From the peak temperatures in Table 2, E_k and E_o, A_k, linear regression coefficient r_k and r_o were obtained and shown in Table 3.

From above the value of the activation energy and the temperature scope of the thermal decomposition in their DSC curves, we can conclude E/RT is more than 20. So the Coats–Redfern equation [10] shown as follows can be cited to obtain the values of E, A and the most probable mechanism function [f(α)].

In this paper, the Coats–Redfern equation is

$$\ln \frac{G(\alpha)}{T^2} = \ln\left(\frac{AR}{\beta E}\right) - \frac{E}{RT} \quad (1)$$

$$G(\alpha) = \int \frac{d\alpha}{f(\alpha)} \quad (2)$$

where G(α) and f(α) are the integral and differential model functions, respectively; R, the gas constant; α, conversion degree ($\alpha = H_t/H_o$); H_o, the total heat effect (corresponding to the global area under the DSC curve); H_t, the reaction heat at a certain time (corresponding to the partial area under the DSC curve); T, temperature (K). The functions of mechanism G(α) [11] in this work are

(1) Avrami-Erofeev nucleation and nucleus growth equation:

$$[-\ln(1-\alpha)]^{(1/n)} \quad (n = 1, 1.5, 2, 3 \text{ and } 4)$$

(2) Diffusion equation:

α^2	(One-dimensional diffusion)
$\alpha + (1-\alpha)\ln(1-\alpha)$	(Valensi Equation)
$[1-(2/3)\alpha] - (1-\alpha)^{(2/3)}$	(Ginstling Brounshtein Equation)
$[1-(1-\alpha)^{(1/3)}]^2$	(Jander Equation)
$[(1+\alpha)^{(1/3)} - 1]^2$	(Anti-Jander Equation)
$[1/(1-\alpha)^{(1/3)} - 1]^2$	(Zhuralev, Lesokin and TemPelman Equation)

(3) Power equation: $\alpha^{1/n}$ (n = 1, 2, 3 and 4).
(4) Chemical reaction of 1, 1.5 and 2 order.
(5) Autocatalysis reaction: $\alpha(1-\alpha)$.

The most probable mechanism function was selected by the better values of r and δ based on the following four conditions: (1) the values of E_a (kJ mol^{-1}) and lg(A (s^{-1})) selected are in the ordinary range of the thermal decomposition kinetic parameters for solid material (E_a (kJ mol^{-1})) = 80–250 and lg(A (s^{-1})) = 7–30; (2) linear correlation coefficient (r) is greater than 0.98; (3) the values of E_a (kJ mol^{-1}) and lg(A (s^{-1})) obtained with the differential and integral methods are approximately the same; (4) the mechanism function selected must be in agreement with the tested sample state.

Kinetic model functions above-mentioned and the data in Table 4 are put into Eqs. (1) and (2) for calculation, respectively. The results of satisfying the above-mentioned condition at

Table 4
The DSC data of BAFF for calculation.

2.5 (K min^{-1})				5 (K min^{-1})				10 (K min^{-1})				20 (K min^{-1})			
T (°C)	α (%)	T (°C)	α (%)	T (°C)	α (%)	T (°C)	α (%)	T (°C)	α (%)	T (°C)	α (%)	T (°C)	α (%)	T (°C)	α (%)
188	0.4474	226	26.43	185	0.1082	216	5.313	198	0.1578	232	7.520	215	0.4553	250	13.79
190	0.6433	228	31.09	186	0.1366	218	6.202	199	0.2027	234	8.765	216	0.5684	252	16.08
192	0.8867	230	36.51	187	0.1723	220	7.259	200	0.2565	236	10.25	217	0.6915	254	18.75
194	1.182	232	42.19	188	0.2116	222	8.519	201	0.318	238	11.98	218	0.8246	256	21.79
196	1.539	234	48.44	189	0.2506	224	10.02	202	0.3912	240	14.05	220	1.119	258	25.21
198	1.941	236	54.88	190	0.2953	226	11.80	204	0.5618	242	6.52	222	1.453	260	29.06
200	2.410	238	61.56	191	0.3548	228	13.92	206	0.7723	244	19.36	224	1.822	262	33.31
202	2.951			192	0.4189	230	16.48	208	1.025	246	22.58	226	2.227	264	38.00
204	3.570			194	0.5784	232	19.46	210	1.333	248	26.26	228	2.664	266	43.12
206	4.311			196	0.7756	234	22.87	212	1.687	250	30.46	230	3.318	268	48.60
208	5.180			198	1.019	236	26.85	214	2.056	252	35.33	232	3.656	270	54.36
210	6.236			200	1.293	238	31.29	216	2.440	254	40.94	234	4.230	272	60.30
212	7.466			202	1.611	240	36.22	218	2.872	256	46.83	236	4.877		
214	8.991			204	1.967	242	41.59	220	3.345	258	52.92	238	5.619		
216	10.82			206	2.369	244	47.45	222	3.841	260	58.98	240	6.479		
218	13.01			208	2.815	246	53.49	224	4.354	261	62.07	242	7.498		
220	15.64			210	3.326	248	59.75	226	4.943			244	8.717		
222	18.79			212	3.895	249	62.84	228	5.640			246	10.16		
224	22.25			214	4.550			230	6.490			248	11.83		

Table 5
The kinetic parameters of BAFF obtained by Coats–Redfern method.

β (K s^{-1})	E_a (kJ mol^{-1})	lg A (s^{-1})	α (%)	r	δ
0.04167	125.58	10.21	0.4474–61.56	0.9988	0.010
0.08333	123.60	10.05	0.1082–62.84	0.9948	0.022
0.16667	120.64	9.73	0.1578–62.07	0.9923	0.025
0.33333	119.02	9.59	0.4553–60.30	0.9966	0.015

Mean: E_a = 122.21 kJ mol^{-1}, lg A = 9.895 s^{-1}, $G(\alpha) = [-\ln(1-\alpha)]^{(1/1.5)}$.

the same time are the final results as listed in Table 5. According to Tables 3 and 5, when $f(\alpha) = (3/2)(1-\alpha)\ [-\ln(1-\alpha)]^{(1/3)}$, $G(\alpha) = [-\ln(1-\alpha)]^{(1/1.5)}$, the values (Table 4) obtained in Eqs. (1) and (2) are in good agreement with the calculated values obtained by the Kissinger's method and Ozawa's method.

So it is reasonable that the most probable mechanism function of the major exothermic decomposition process for BAFF is $f(\alpha) = (3/2)(1-\alpha)\ [-\ln(1-\alpha)]^{(1/3)}$, its integral form is $G(\alpha) = [-\ln(1-\alpha)]^{(1/1.5)}$, the apparent activation energy E_a is 122.21 kJ mol^{-1}, the pre-exponential factor A is $10^{9.89}$ s^{-1}. The results indicate that the decomposition mechanism of the major exothermic decomposition process of BAFF belongs to "nucleation and nucleus growth" obeys the equation of Avrami-Erofeev with $n = 1.5$. Substituting the differential form of the most probable mechanism function $G(\alpha)$ with $[-\ln(1-\alpha)]^{(1/1.5)}$, the apparent activation energy E_a with 122.21 kJ mol^{-1} and the pre-exponential factor A with 109.89 s^{-1} in the non-isothermal kinetics equation, one can establish the kinetics equation of the major exothermic decomposition process for BAFF as follows:

$$\frac{d\alpha}{dt} = 10^{10.07} \exp(-1.46993 \times 10^4/T)(1-\alpha)[-\ln(1-\alpha)]^{1/3} \quad (3)$$

3.4. Thermal decomposition mechanism

Thermolysis/RSFT-IR was used to measure the condensed phase products of the thermal decomposition of BAFF under the linear heating condition in real time. The infrared spectra of BAFF at different temperature are shown in Fig. 3.

It can be clearly seen from Fig. 3 that the two peaks in 1634 cm^{-1} and 1610 cm^{-1} merge into a peak at 160 °C, which is resulted by the solid–liquid phase transition of BAFF. The fact that the CO_2 IR absorption band comes out at 188 °C suggests the initiation of BAFF decomposition. The temperature observing the CO_2 IR absorption band approaches to the initia1 temperature of BAFF decomposition on TG curve. IR absorption bands of 1463 cm^{-1} and 990 cm^{-1}, 964 cm^{-1} at 325 °C suggest the cleavage of furoxan ring. IR absorption bands of 1635 cm^{-1}, 1338 cm^{-1} and 1560 cm^{-1} are respectively υ (C=N → O) and υ (C=N) vibration. The weakened IR absorption bands υ (C–NH_2) in 3462 cm^{-1}, 3332 cm^{-1}, υ (C=N → O) and υ (C=N) became gradually broad and move to low frequency from 325 °C to 503 °C. There is the obvious IR absorption band of $NH_4[N(CN)_2]$ in 2165 cm^{-1} at 440 °C.

The absorption IR spectra of the solid residue from thermolysis of BAFF are shown in Fig. 4 and are compared with the spectrum of pure melamine. Except the IR absorption bands of CO_2 (2352 cm^{-1} and 670 cm^{-1}) and $NH_4[N(CN)_2]$ (2165 cm^{-1}), the match is very good in the 1750–750 cm^{-1} range. These melamine and melamine-like products form in the condensed phase probably without passing through the cyanamide (NH_2CN) because there is no characteristic absorption of NH_2CN in Fig. 4. "When NH_2CN forms it is able to vaporize even at pressure up to 6.895 MPa Ar. Hence, if free NH_2CN was an important intermediate it would have been detected by IR [12]".

Fast thermolysis/RSFT-IR was used to measure the real-time gas products of thermal decomposition of BAFF under high heating rate conditions (T-jump/RSFT-IR test), high heating rate conditions are

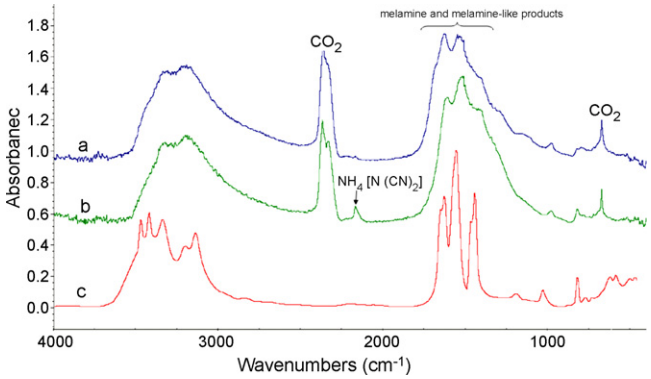

Fig. 4. Comparison of the IR spectra of the solid residue from thermolysis of BAFF with that of pure melamine. (a) The solid residue from thermolysis of BAFF at 403 °C under the linear temperature increment condition. (b) The solid residue from thermolysis of BAFF at 503 °C under the linear temperature increment condition. (c) Pure melamine.

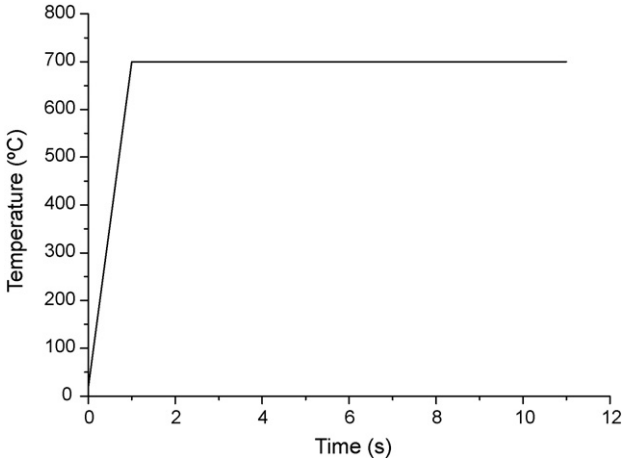

Fig. 5. High heating rate curve of T-jump/RSFT-IR test.

shown in Fig. 5. The IR spectra of gaseous products are shown in Fig. 6.

The IR absorption bands of 844 cm^{-1}, 1025 cm^{-1}, 1164 cm^{-1}, 1210 cm^{-1}, 1276 cm^{-1}, 1330 cm^{-1}, 1442 cm^{-1}, 1596 cm^{-1}, etc. on the fast thermolysis/RSFT-IR spectra should be attributed to gaseous BAFF.

From Fig. 6, some new IR absorption bands come out on the IR spectra of the gaseous products of BAFF decomposition. These absorption bands indicate that the detected decomposition products of BAFF consist of CO_2 (2363 cm^{-1}, 2323 cm^{-1} and 670 cm^{-1}), NO_2 (1627 cm^{-1}), NO (1908 cm^{-1} and 1847 cm^{-1}), N_2O (2240 cm^{-1}). There are not the absorption bands of NH_3.

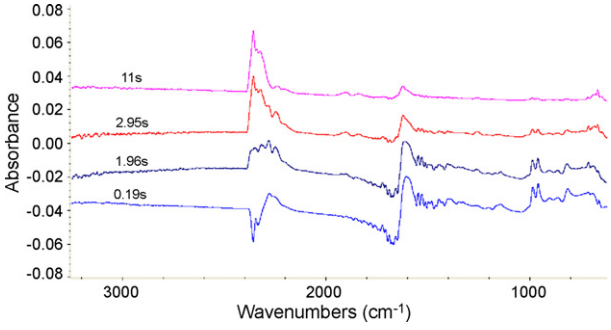

Fig. 6. IR spectra of the gaseous products for thermolysis of BAFF at different time.

In general, the thermal decomposition of furazans and furoxans leads to the formation of nitriles and nitrile-oxides [13]. However, some furazans such as 3,4-diaminofurazan (DAF) liberate gaseous products, but also produce cyclic azine polymers [14]. BAFF is an example of such compounds. According to the above study, the cleavage of furoxan ring in the BAFF is first, the structure of free radical of aminofurazan is similar with DAF and the absorption IR spectra of the solid residue from thermolysis of BAFF are similar with that of DAF, so the mechanism of decomposition of BAFF can be forecasted as given below:

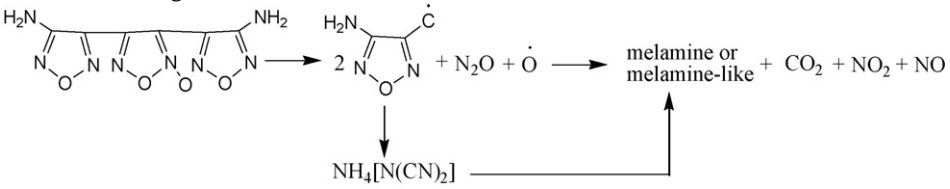

4. Conclusions

(1) The melting point of BAFF is 168.4 °C. The temperature range of BAFF major exothermic decomposition is 181–290 °C, and the decomposition process of BAFF can be divided into two stages, the first stage include the two steps of mass loss. The peak temperatures of the two exothermic peaks are 260.4 °C and 338.8 °C at ambient pressure on DSC curve, respectively.

(2) The apparent activation energy E_a is 122.21 kJ mol^{-1}, the pre-exponential factor A is $10^{9.89}$ s^{-1}. The most probable mechanism function indicates that the decomposition kinetics equation of BAFF belongs to"nucleation and nucleus growth" and obeys the equation of Avrami-Erofeev with $n = 1.5$. The kinetics equation of exothermic decomposition for the major exothermic decomposition process of BAFF is $d\alpha/dt = 10^{10.07} \exp(-1.46993 \times 10^4/T)(1-\alpha)[-\ln(1-\alpha)]^{1/3}$.

(3) The thermal decomposition products of BAFF consist not only of gaseous products CO_2, NO_2, N_2O, NO, but also of condensed products ammonium dicyanamide ($NH_4[N(CN)_2]$), cyclic azines (melamine or melamine-like).

Acknowledgment

It is a pleasure to acknowledge my appreciation to Professor Liu Zi-ru who has revised my paper and advised many valuable suggestions.

References

[1] T.S. Nivikova, T.M. Mei Nikowa, O.V. Kharitonova, et al., An effective method for the oxidation of aminofurazans to nitrofurazans, Mendeleev Communication 4 (1994) 139–140.
[2] A.B. Sheremeteev, Chemistry of furazan fused to five-membered rings, Journal of Heterocyclic Chemistry 32 (1995) 371–385.
[3] Z. De-xiong, Z. Yan, W. Qi, Advances in high energy density matter of furazan series, Journal of Solid Rocket Technology 27 (2004) 32–36.
[4] Z. Fengqi, C. Pei, H. Rongzu, Thermochemical properties and non-isothermal decomposition reaction kinetics of 3,4-dinitrofurazanfuroxan (DNTF), Journal of Hazardous Materials A113 (2004) 67–71.
[5] H. Huanxing, Z. Zhizhong, Z. Fengqi, et al., A study on the properties and application of high energy density material DNTF, Acta Armamentarh 25 (2004) 155–158.
[6] Z. Yan-shui, L. Jian-kang, H. Xin-ping, et al., Synthesis and properties of 3,4-bis(4′-aminofurazano-3′) furoxan, Chinese Journal of Explosive & Propellant 30 (2007) 54–56.
[7] W. Jun, L. Jinshan, L. Qinqin, et al., A novel insensitive high explosive 3,4-bis(4′-aminofurazano-3′) furoxan, Propellants, Explosives, Pyrotechnics 5 (2008) 347–352.
[8] H.E. Kissinger, Reaction kinetics in differential thermal analysis, Analytical Chemistry 29 (1957) 1702–1706.
[9] T. Ozawa, A new method of analyzing thermogravimetric data, Journal of Bulletin of the Chemical Society of Japan 38 (1) (1965) 1881–1886.
[10] A.W. Coats, J.P. Redfern, Kinetic parameters from thermogravimetric data, Nature 201 (1964) 68–69.
[11] L. Zi-ru, Thermal Analyses for Energetic Materials, National Defence Industry Press, Beijing, 2009, pp.59–63.
[12] A. Gao, Y. Oyumi, T.B. Brill, Thermal decomposition of energetic materials 49. Thermolysis routes of mono- and diaminotetrazoles, Combustion and Flame 83 (1991) 345–352.
[13] G.B. Manelis, G.M. Nazin, Y.I. Rubtsov, V.A. Strunin, Thermal Decomposition and Combustion of Explosives and Propellants, Taylor & Francis Group, London and New York, 2003, pp.113–125.
[14] C.E. Stoner, T.B. Brill, Thermal decomposition of energetic materials 46. The formation of melamine-like cyclic azines as a mechanism for ballistic modification of composite propellants by DCD, DAG and DAF, Combustion and Flame 83 (1991) 302–308.